Discrete Particle Simulation of Gas Fluidization of Particle Mixtures

Y. Q. Feng, B. H. Xu, S. J. Zhang, and A. B. Yu
Centre for Simulation and Modeling of Particulate Systems, School of Materials Science and Engineering, The University of New South Wales, Sydney, NSW 2052, Australia

P. Zulli
BHP Steel Research Laboratories, Port Kembla, NSW 2505, Australia

DOI 10.1002/aic.10169
Published online in Wiley InterScience (www.interscience.wiley.com).

This report presents a numerical study of segregation and mixing of binary mixtures of particles in a gas-fluidized bed by means of discrete particle simulation, where the motion of individual particles is 3-D and the flow of continuous gas is 2-D. Periodic boundary conditions are applied to the front and rear walls to represent a bed of large thickness with a relatively small number of particles. Two initial packing conditions are used in this simulation: completely separated, with the flotsam (1×10^{-3} m in diameter) on the top of the jetsam (2×10^{-3} m in diameter), and well mixed. The flotsam and jetsam are of the same density, with each counting 50% in weight. Gas is injected uniformly at the bottom. Two superficial gas velocities, 1.0 and 1.4 m/s, are used in the simulation, producing significant segregation and good mixing, respectively. The results show that the degree and rate of segregation or mixing are significantly affected by gas velocity and the final equilibrium states are not affected by the initial packing states for a given gas velocity. Significant segregation occurs at a gas velocity of 1.0 m/s, with the top fluidized layer rich in flotsam and the bottom defluidized layer rich in jetsam, whereas there was less segregation at 1.4 m/s with most of the bed fluidized. The simulated results are qualitatively comparable with those observed in the physical experiments conducted under similar conditions. On this basis, the mixing kinetics obtained from the numerical simulation is quantified with a weighted Lacey mixing index and explained in terms of microdynamic results in relation to particle–particle and particle–fluid interactions. It is proposed that an appropriate sampling size should be able to describe properly the two extremes: well mixed and fully segregated. The results also demonstrate that size segregation occurs as a result of the strong fluid drag force lifting the flotsam before a dynamical equilibrium is reached, and the particle–particle interaction, like the particle–fluid interaction, plays an important role in achieving uniform fluidization. © 2004 American Institute of Chemical Engineers *AIChE J,* 50: 1713–1728, 2004

Keywords: fluidization, mixing, size segregation, gas–solid flow, binary mixture, discrete particle simulation

Introduction

Segregation of solids may be found when particles with different shapes, sizes, and/or densities are fluidized by gas. Its occurrence can be either detrimental or beneficial, depending on specific applications. Good solid mixing is desired in situations such as coal combustion, whereas segregation is needed to separate one solid from the other. The knowledge of the fundamentals governing segregation or mixing is important for better using these phenomena to enhance the performance of operations. Therefore it has been a continuous subject of research.

Correspondence concerning this article should be addressed to A. B. Yu at a.yu@unsw.edu.au.

Previous studies have shown that many variables affect the mixing/segregation behavior, including particle properties such as particle size, density, and shape, and operational conditions such as superficial gas velocity, particle concentration, initial packing condition, and bed aspect ratio. Some general knowledge about their effects has been obtained. For example, it is known that segregation is most significant at superficial gas velocities between the minimum fluidization velocities of flotsam (smaller or lighter particles) and jetsam (larger or heavier particles), and correlations have been formulated for calculating the minimum fluidization velocity of binary mixtures (see, for example, Wu and Baeyens, 1998); density difference is more significant than size difference (Rowe et al., 1972); segregation is more pronounced for a bed of low aspect ratio (Formisani et al., 2001; Wu and Baeyens, 1998). The mixing index, as an important parameter to quantify the kinetics of the process, is usually studied by the bed freeze and dissection method, which is very laborious and suffers a great deal of uncertainty. Some empirical or semiempirical correlations and theoretical models have been proposed to predict this phenomenon (Beeckmans, 1984; Gibilaro and Rowe, 1974; Hoffmann et al., 1993; Nienow et al., 1978; Shen and Zhang, 1998). However, because of the complexity of the problem, in practice these models are not reliable for general application.

Segregation as a bulk behavior results from the collective interactions among individual particles, in addition to the interaction between gas and particles. Therefore, analysis on a particle scale based on information such as the trajectories of, and forces acting on, individual particles are critical to the elucidation of the governing mechanisms of mixing/segregation. Gas fluidization involves strong coupling between discrete particles and continuum gas, and is a very complicated dynamic process with vigorous temporal and spatial variation. At this stage of development, it is not possible to generate experimental information rich enough for particle-scale analysis. For example, the newly developed positron emission particle tracking (PEPT) technique can trace only one or several particles, based on which to derive the velocity field of particles in a fluidized bed (Hoomans et al., 2001; Stein et al., 1995; Stewart et al., 2001). However, other dynamic information, such as transient flow structure and forces of particles, is still unavailable. The lack of quantitative particle-scale information has hindered the development of a general method for reliable scale-up, design, and control/optimization of mixing/segregation behaviors. In recent years, numerical methods have been developed to overcome this difficulty. This is mainly achieved by combining the discrete particle method (DPM) for solid phase with computational fluid dynamics (CFD) for gas phase, that is, the so-called DPM-CFD approach (Tsuji et al., 1993; Xu and Yu, 1997).

In such a model, the motion of individual particles is obtained by solving Newton's second law of motion, whereas fluid flow is obtained by solving the Navier–Stokes equations with their coupling by Newton's third law of motion. This approach can generate detailed information about the trajectories of particles and the transient forces between particles and between particle and fluid, thereby providing a promising way to probe the underpinning physics of gas–solid flow, as discussed by Yu and Xu (2003). The usefulness of this approach has been proved from its success in quantifying the effects of variables, such as materials properties (Hoomans et al., 1998) and cohesive forces (Kuwagi et al., 2000; Mikami et al., 1998; Rhodes et al., 2001a; Xu and Yu, 2001), in the microdynamic analysis of gas fluidization (Xu and Yu, 1998; Xu et al., 2002) or examination of the performance of complex flow systems involving inserts (Kawaguchi et al., 1998; Rong et al., 1999), elevated pressure (Li and Kuipers, 2002), heat transfer (Li and Mason, 2000), or chemical reaction (Kaneko et al., 1999). Various phenomena associated with gas–solid flow have been simulated by this method, including spouting, bubbling, slugging and clustering behavior, cavity formation, and bed expansion (Helland et al., 2000; Kawaguchi et al., 2000; Ouyang and Li, 1999; Xu and Yu, 2002; Xu et al., 2000; Yuu et al., 2000). However, almost all the DPM-CFD studies reported are conducted using two-dimensional (2-D) or pseudo 3-D beds with monosized particles. In the former case, disks are used and in the latter case, bed thickness is the same as the diameter of particles. Segregation of binary mixtures has been studied by a 2-D approach, in which particles are treated as different sized discs (Hoomans et al., 2000). The porosity calculated in 2-D needs to be transferred to the one in three dimension through an arbitrary treatment. Furthermore, segregation attributed to interparticle percolation is considerably suppressed because of the loss of 1-D motion.

This report presents a numerical study of segregation and mixing of binary mixtures of particles in a gas-fluidized bed by means of discrete particle simulation where the motion of individual particles is three-dimensional and the flow of continuous gas is two-dimensional. The focuses are on the effects of two variables: the initial packing state and gas velocity. The validity of the approach is examined by comparing the simulated and measured results under comparable conditions in terms of solid flow pattern. Based on the simulated results, the mixing/segregation kinetics and the role of particle–particle and particle–fluid interactions are analyzed in detail.

Simulation Method

Governing equations

The formulation of governing equations is in principle the same as the one used by Xu and Yu (1997, 2000). Development has been made to consider multisized particles and 3-D solid flow in a fluidized bed, and is briefly outlined as follows.

The solid phase is treated as a discrete phase that is described by a conventional discrete element method (DEM), originally proposed by Cundall and Strack (1979), and has been widely accepted as a most powerful DPM technique in granular research (see, for example, Thornton, 2000). Thus, the translational and rotational motions of a particle at any time t, in a bed, are determined by Newton's second law of motion, which can be written as

$$m_i \frac{d\mathbf{v}_i}{dt} = \mathbf{f}_{f,i} + \sum_{j=1}^{k_i} (\mathbf{f}_{c,ij} + \mathbf{f}_{d,ij}) + \mathbf{f}_{g,i} \tag{1}$$

and

$$I_i \frac{d\boldsymbol{\omega}_i}{dt} = \sum_{j=1}^{k_i} \mathbf{T}_{ij} \tag{2}$$

Table 1. Components of Forces and Torque Acting on Particle *i*

Forces and Torque	Symbol	Equation*
Normal forces		
Contact	$\mathbf{f}_{cn,ij}$	$-\frac{4}{3}E^*\sqrt{R^*}\,\delta_n^{3/2}\mathbf{n}$
Damping	$\mathbf{f}_{dn,ij}$	$-\eta_n(6m_{ij}E^*\sqrt{R^*\delta_n})^{1/2}\mathbf{v}_{n,ij}$
Tangential forces		
Contact	$\mathbf{f}_{ct,ij}$	$-\frac{\mu_s\mathbf{f}_{cn,ij}}{\lvert\boldsymbol{\delta}_{t,ij}\rvert}\left[1-\left(1-\frac{\min\{\lvert\delta_{t,ij}\rvert,\,\delta_{t,ij,\max}\}}{\delta_{t,ij,\max}}\right)^{3/2}\right]\boldsymbol{\delta}_{t,ij}$
Damping	$\mathbf{f}_{dt,ij}$	$-\eta_t\left(6m_{ij}\mu_s\mathbf{f}_{cn,ij}\frac{\sqrt{1-\delta_{t,ij}/\delta_{t,ij,\max}}}{\delta_{t,ij,\max}}\right)^{1/2}\mathbf{v}_{t,ij}$
Fluid drag force	$\mathbf{f}_{f,i}$	$0.5c_{d0,i}\rho_f\pi R_i^2\lvert\mathbf{u}_i-\mathbf{v}_i\rvert(\mathbf{u}_i-\mathbf{v}_i)\varepsilon_i^{1-\chi}$
Torque	$\mathbf{T}_{i,j}$	$\mathbf{R}_i\times(\mathbf{f}_{ct,ij}+\mathbf{f}_{dt,ij})$
Gravity	$\mathbf{f}_{g,i}$	$m_j\mathbf{g}$

*where:

$$\frac{1}{R^*}=\frac{1}{R_i}+\frac{1}{R_j},\ E^*=\frac{E}{2(1-\nu^2)},\ \mathbf{n}=\frac{\mathbf{R}_i}{R_i},\ \delta_{t,ij,\max}=\mu_s\frac{2-\nu}{2(1-\nu)}\delta_n,\ m_{ij}=\mathbf{v}_{ij}=\mathbf{v}_j-\mathbf{v}_i+\boldsymbol{\omega}_j\times\mathbf{R}_j-\boldsymbol{\omega}_i\times\mathbf{R}_i,\ \mathbf{v}_{n,ij}=(\mathbf{v}_{ij}\cdot\mathbf{n})\cdot\mathbf{n},\ \mathbf{v}_{t,ij}=(\mathbf{v}_{ij}\times\mathbf{n})\times\mathbf{n},$$

$$c_{d0,i}=\left(0.63+\frac{4.8}{\mathrm{Re}_{p,i}^{0.5}}\right)^2,\ \mathrm{Re}_{p,i}=\frac{2\rho_f R_i\varepsilon_i\lvert\mathbf{u}_i-\mathbf{v}_i\rvert}{\mu_f},\ \boldsymbol{\chi}=3.7-0.65\exp\left[-\frac{(1.5-\log_{10}\mathrm{Re}_{p,i})^2}{2}\right]$$

where m_i, I_i, k_i, $\mathbf{v}_i$, and $\boldsymbol{\omega}_i$ are, respectively, the mass, momentum of rotational inertia, number of contacting particles, and translational and rotational velocities of particle i; $\mathbf{f}_{f,i}$ and $\mathbf{f}_{g,i}$ are fluid drag force and gravitational force, respectively; and $\mathbf{f}_{c,ij}$, $\mathbf{f}_{d,ij}$, and $\mathbf{T}_{i,j}$ are the contact force, viscous contact damping force, and torque between particles i and j. These interparticle forces and torques are summed over the k_i particles in contact with particle i.

The particle–particle and particle–wall contact force is calculated based on a soft-sphere method. The particle fluid interaction force is calculated according to the correlation by Di Felice (1994), which has been used by Xu and Yu (1997, 2000) and Kafui et al. (2002). The equation is initially formulated for monosized particles. Because it is based on the analysis of a single particle, conceptually it can be directly applied to multisized particles, although its accuracy may need to be examined. The formulations used to calculate the forces and torques involved in Eqs. 1 and 2 are listed in Table 1. These equations, or the like, have been extensively used in our study of particle packing and flow related to various industrial processes as recently summarized by Yu (2002).

The gas phase is treated as a continuous phase and modeled in a way very much similar to the one widely used in the conventional two-fluid modeling (see, for example, Gidaspow, 1994). Thus, its governing equations are the conservations of mass and momentum in terms of the local mean variables over a computational cell, given by

$$\frac{\partial\varepsilon}{\partial t}+\nabla\cdot(\varepsilon\mathbf{u})=0 \tag{3}$$

and

$$\frac{\partial(\rho_f\varepsilon\mathbf{u})}{\partial t}+\nabla\cdot(\rho_f\varepsilon\mathbf{u}\mathbf{u})=-\nabla P-\frac{\sum_{i=1}^{k_c}\mathbf{f}_{f,i}}{\Delta V}+\nabla(\varepsilon\boldsymbol{\tau})+\rho_f\varepsilon\mathbf{g} \tag{4}$$

where ρ_f, $\mathbf{u}$, and P are, respectively, the fluid density, velocity, and pressure; $\boldsymbol{\tau}$, ϵ, and ΔV are the fluid viscous stress tensor, porosity, and volume of a computational cell, respectively.

Obviously, the modeling of the solid flow by DEM is at the individual particle level, whereas the gas flow by CFD is at the computational cell level. Their coupling is numerically achieved as follows. At each time step, DEM will give information, such as the positions and velocities of individual particles, for the evaluation of porosity and volumetric fluid drag force in a computational cell. CFD will then use these data to determine the gas flow field, which then yields the fluid drag

Table 2. Parameters Used in the Present Simulations

Particle Phase			Gas Phase		
Density (kg m^{-3})		2500	Viscosity (kg m^{-1} s^{-1})		1.8×10^{-5}
Young's modulus (Nm^{-2})		1.0×10^{8}	Density (kg m^{-3})		1.205
Poisson ratio (Nm^{-2})		0.3	CFD cell	Width (m)	0.00325
Sliding friction coefficient		0.3		Height (m)	0.00325
Damping coefficient		0.2	Bed geometry	Width (m)	0.065
Particle diameter (m)	Flotsam	0.001		Height (m)	0.26
	Jetsam	0.002		Thickness (m)	0.0081
Number of particles	Flotsam	22,223	Bed distributor		Uniform
	Jetsam	2777			
Time step (s)		2.5×10^{-6}	Time step (s)		2.5×10^{-6}

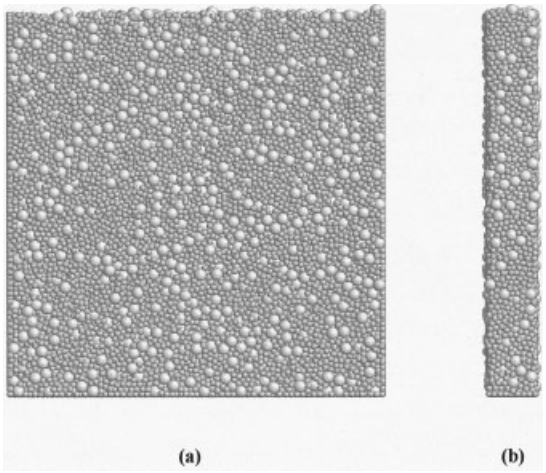

Figure 1. Initial (well mixed) packing state: (a) front view; (b) side view.

forces acting on individual particles. Incorporation of the resulting forces into DEM will produce information about the motion of individual particles for the next time step. The fluid drag force acting on individual particles will react on the fluid phase from the particles, so that Newton's third law of motion is satisfied. The advantage of this coupling technique has been discussed in previous work (see, for example, Xu and Yu, 1997; Yu and Xu, 2003).

Equations 1 and 2 for particle flow can be numerically solved by an explicit time integration method, facilitated with suitable boundary conditions for given flow conditions. Here, the interparticle force models are also applied to the interaction between a particle and a wall, with the corresponding wall properties used. However, the wall is assumed to be so rigid that no displacement and movement result from this interaction. On the other hand, Eqs. 3 and 4 for gas flow can be readily solved by use of a conventional CFD method (Zhang and Yu, 2002; Zhang et al., 1998). For the present simulation, a no-slip boundary condition is applied to bed walls and zero normal

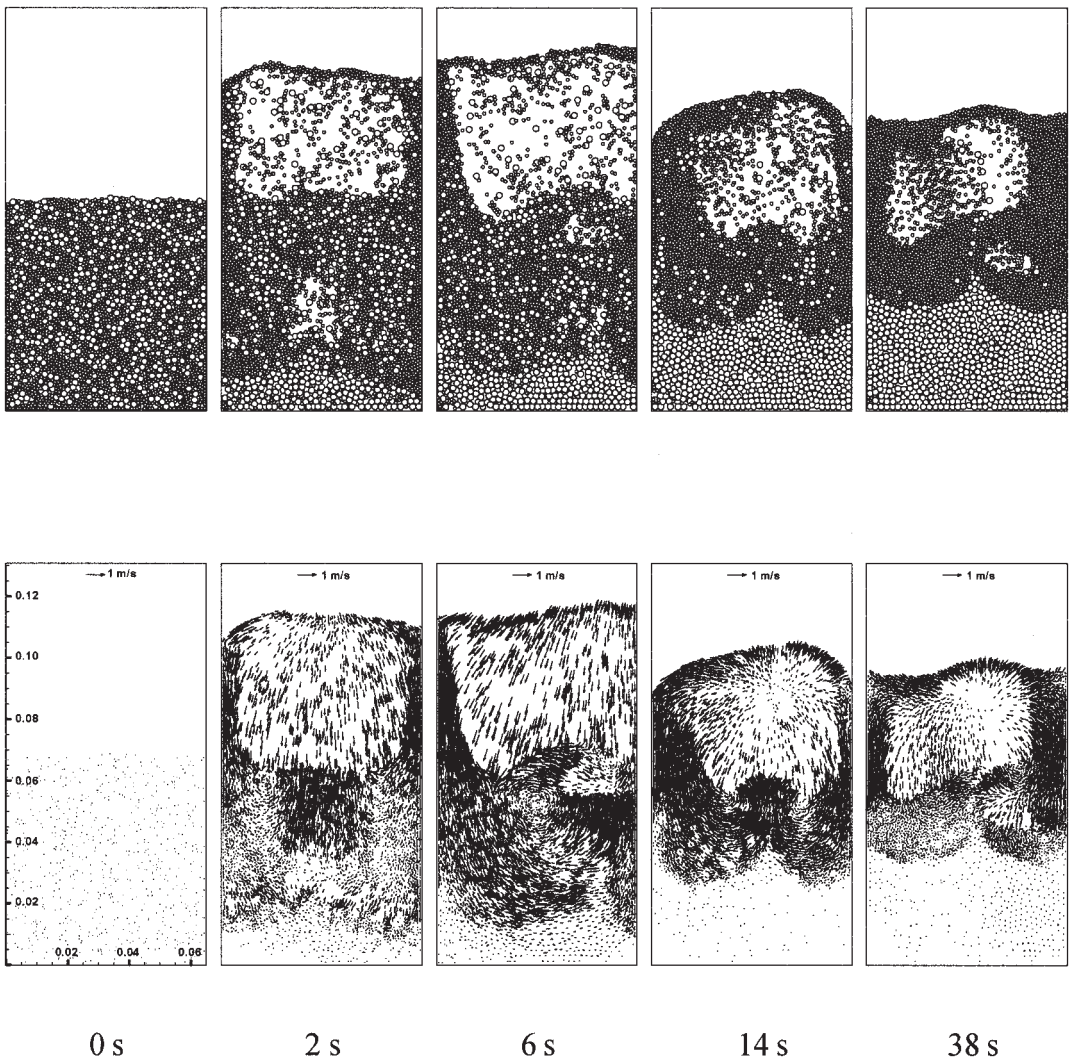

Figure 2. Particle configuration (top) and velocity field (bottom) at different times for a bed whose initial state is well mixed, when superficial gas velocity is at 1.0 m/s.

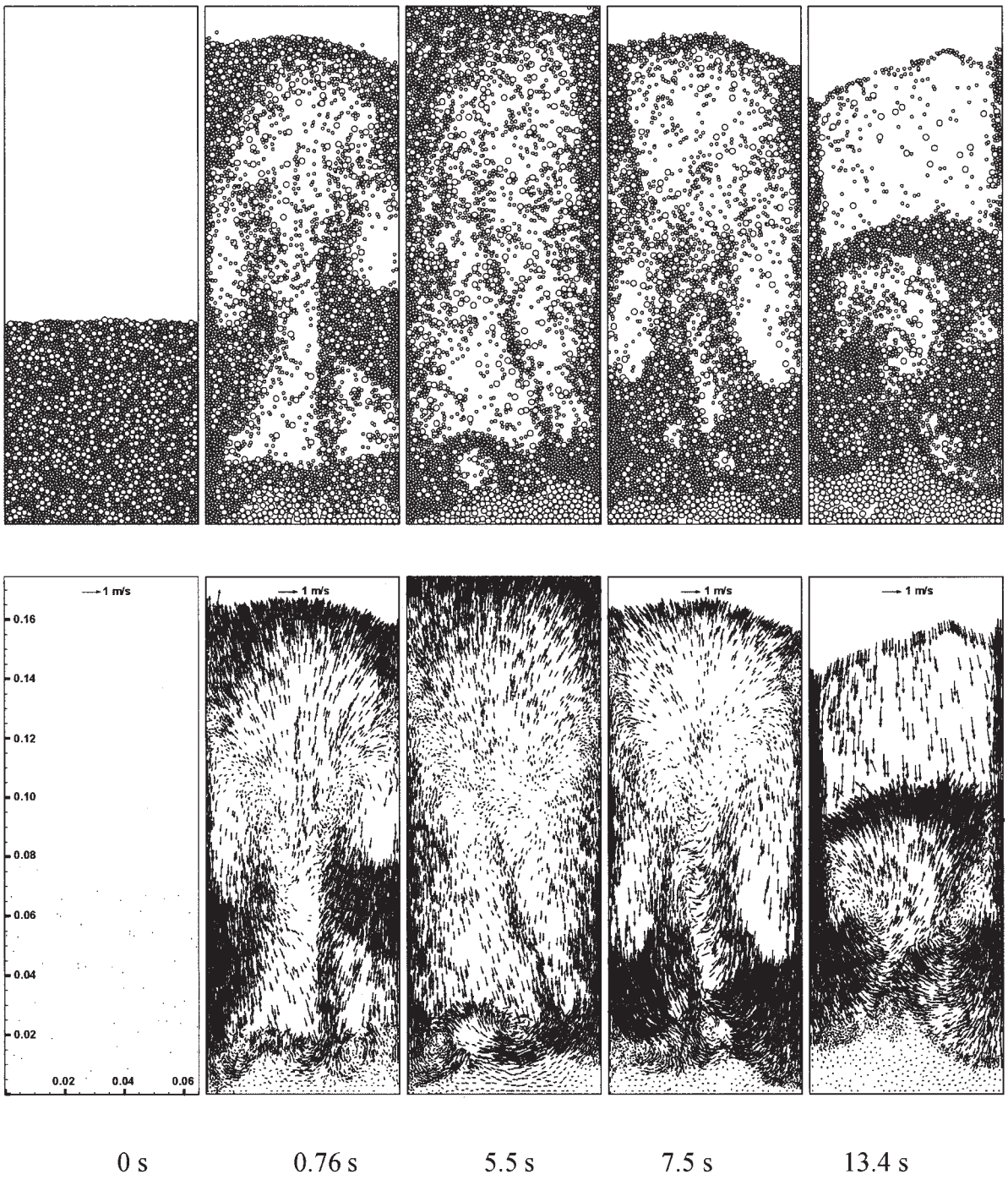

Figure 3. Particle configuration (top) and velocity field (bottom) at different times for a bed whose initial state is well mixed, when superficial gas velocity is at 1.4 m/s.

gradient condition to the top exit for gas velocity; the gas flow at inlet is specified.

Simulation conditions

Table 2 shows the parameters used in this simulation. Spherical particles are used as the solid phase fluidized in a rectangular bed. Periodical boundary conditions are applied to the front and rear walls for this phase. This treatment can effectively reduce the wall effect imposed by the front and rear walls and allow the 3-D motion of particles in the bed with a relatively small number of particles (Yang et al., 2001). The flow of gas is assumed to be two-dimensional, given that the bed width is much larger than its thickness.

A simulation is started with the random generation of particles without overlaps in the rectangular bed, followed by a gravitational settling process for 0.6 s. Then, gas is uniformly injected at the bottom to fluidize the bed. Two initial packing states are used in this work: well mixed and fully segregated,

with flotsam on the top of the jetsam. The top surface of the packed particles after settling is about 6.5×10^{-2} m high, almost the same as the bed width. Figure 1 shows the front and side views of the well-mixed initial packing. After some trials, two gas velocities, 1.0 and 1.4 m/s, are selected in this work, which respectively produce significant segregation and good mixing. The results are used to elucidate the underlying mechanisms.

Results and Discussion

Solid flow patterns

Figure 2 shows the particle configurations and velocity distributions at different times, when the superficial gas injection velocity is 1.0 m/s. For better visualization, only particles whose center points are between 1.5×10^{-3} and 2.5×10^{-3} m in the thickness direction are presented (this applies to all figures illustrating flow patterns in this work). Once gas is introduced into the bed, segregation appears gradually with jetsam aggregated at the bottom layer. Finally, two layers can be identified. The top layer, rich in flotsam, is in the fluidized state, and the bottom layer, rich in jetsam, is in the defluidized state. It can be observed that the bubbles and slugs, initiated above the interface between jetsam and flotsam, lift the underneath jetsams up through the wakes, producing a mixing process. In the meantime, the jetsam will preferentially move down the bed as a bubble flows up, producing a segregation process. After a period of about 20 s, a dynamic equilibrium is reached where the mixing and segregation processes are balanced. A clear interface can be seen between the two layers. The interface between the two layers surges like a wave, corresponding to the crunch of the interface particles agitated by the bubbles and slugs initiated around the interface, and a wave peak is generated by a bubble or slug drifting the bottom jetsam up. There are always some jetsam particles in the fluidized layer, attributed to the flow of such bubbles and slugs, and some flotsam percolating in the defluidized layer. Therefore, perfect segregation is not possible.

When gas injection velocity is increased to 1.4 m/s, as shown in Figure 3, both jetsam and flotsam are fluidized with bubbles and slugs continuously rising through the bed and bursting out at the bed surface. The motion of particles is much more vigorous than that at the lower gas velocity. Consequently, its dynamic equilibrium can be established quickly and with less segregation.

The segregation at the two velocities can be quantified in terms of the vertical distribution of mass fraction of jetsam. The positions of particles are recorded every 0.02 s in a simulation. Fluctuation is significant because of the vigorous flow of gas and particles but can be eliminated largely by time-averaging. Figure 4 shows the results obtained by averaging 50 records for each point. The results correspond to those observed in Figures 2 and 3 but are more quantitative.

Figure 5 shows the solid flow patterns from a fully segregated bed when the superficial gas velocity is 1.0 m/s. Starting from the completely segregated state, the flotsam in the top part is fluidized with bubbles and slugs, and the jetsam in the bottom part remains defluidized. The jetsam adjacent to the flotsam can be dragged to the upper part of the bed by the wake of bubbles and slugs (mixing process) and move down through

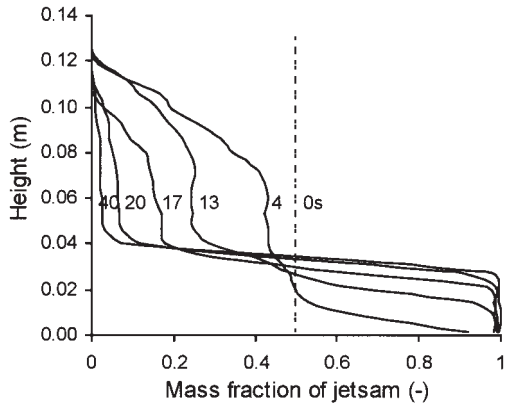

(a)

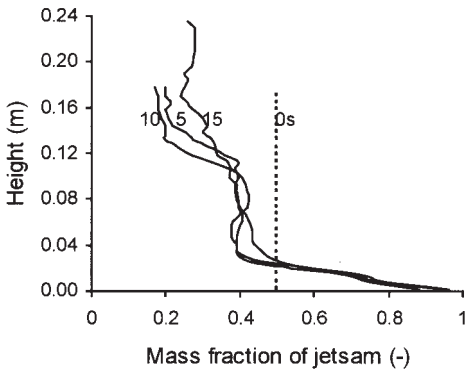

(b)

Figure 4. Mass fraction distribution of jetsam at vertical direction at different times at different superficial gas velocities when the initial state is well mixed: (a) v = 1.0 m/s; (b) v = 1.4 m/s.

the flotsam (segregation process). After a period of rearrangement, a dynamic equilibrium state is achieved, where the mixing process balances the segregation process. When the superficial gas velocity is increased to 1.4 m/s, as shown in Figure 6, the whole bed is fluidized, the vigorous bubbling and slugging produce a better mixing state, with limited segregation at the bottom. Comparison of the results in Figures 2 and 5, or 3 and 6, indicates that the final equilibrium state is not sensitive to the initial packing of particles, which will be further confirmed in our later analysis of the mixing kinetics.

To develop a confidence about the proposed approach, physical experiments were conducted under conditions comparable to those used in the simulation. The bed thickness is also 4.05 times the jetsam diameter; however, the front and rear walls have to be used to support particles. The wall is made of Perspex sheet. Glass beads of diameters 1 and 2×10^{-3} m are used for the solid phase and air for the gas phase. A segrega-

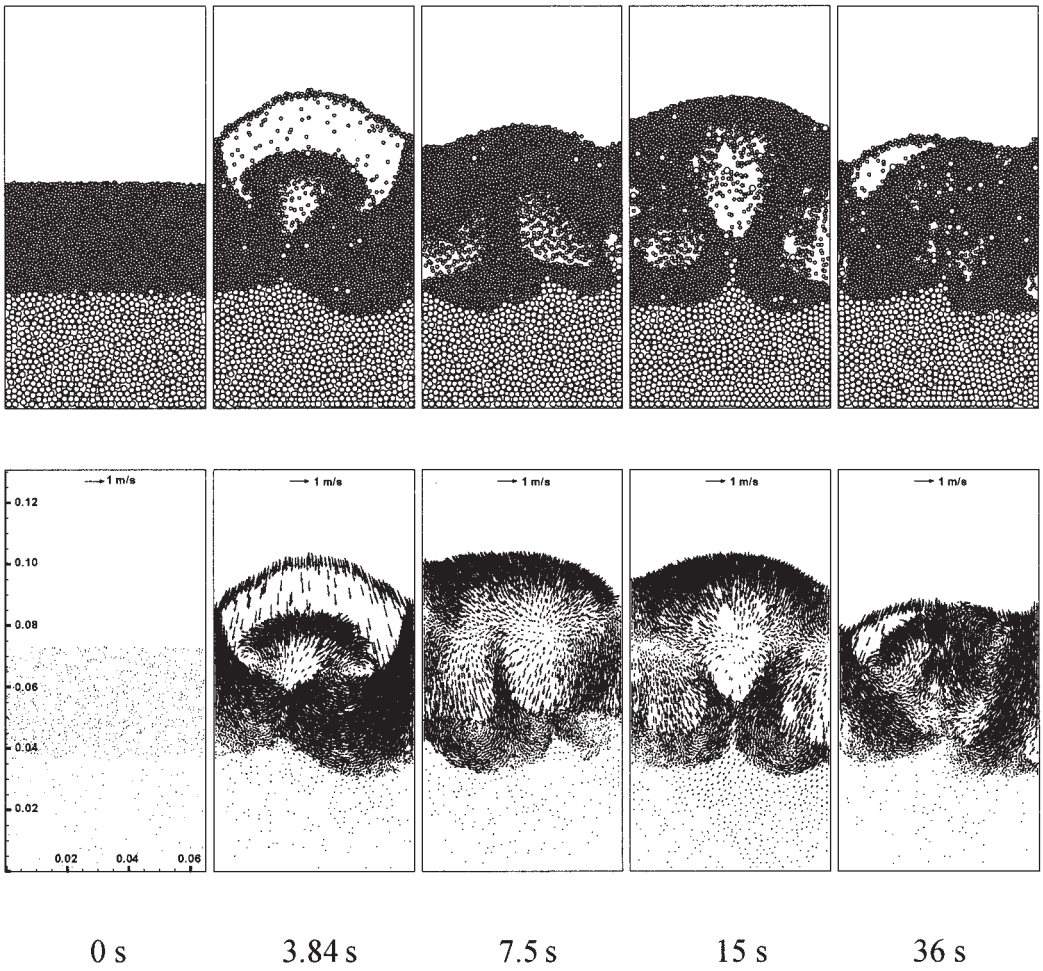

Figure 5. Particle configuration (top) and velocity field (bottom) at different times for a bed whose initial state is fully segregated, when superficial gas velocity is at 1.0 m/s.

tion/mixing process is recorded by a digital video camera. Different sized particles can be identified by the colors reflected through light (dark for flotsam and bright for jetsam). Figure 7 shows the solid flow patterns measured. Obviously, the results from the physical and numerical experiments are quite comparable. Perfect segregation or mixing is not possible under the present flow conditions. For example, the measured and simulated results both indicate that, although both flotsam and jetsam are fluidized at high gas velocities, there are always some jetsam particles simply moving on the bottom plate of the bed. Note that the conditions for physical and numerical experiments are not exactly the same. For example, front and rear walls are present in the physical experiment, whereas the use of a periodical boundary condition in the numerical experiment means the gap between the front and rear walls is infinitely large. The parameters selected for simulation may not fully represent the materials properties for experiment. Thus, the comparison between physical and numerical experiments is qualitative. Nonetheless, it confirms that the present model has captured the key features of this gas–solid flow system. On this basis, further analysis was made with the simulated results, as discussed below.

Mixing kinetics

Different mixing indices have been proposed to quantify the degree of mixing/segregation (see, for example, Hemiti et al., 1990; Lacey, 1954; Nienow et al., 1987; Rice and Brainovich, 1986). An extensive discussion of different forms of mixing indices, as well as sampling size and method for binary mixture, has been made by Fan et al. (1970) and, more recently, Poux et al. (1991), respectively. To date, it remains an active research topic (Rollins et al., 1995). For simplicity, the present analysis is based on the so-called Lacey mixing index (Lacey, 1954), which can be given by

$$M = \frac{S_0^2 - S^2}{S_0^2 - S_R^2} \tag{5}$$

where S^2 is the actual variance, S_0^2 and S_R^2, respectively, represent the variances of the completely segregated and well mixed states, given by

$$S_0^2 = p \cdot q \tag{6}$$

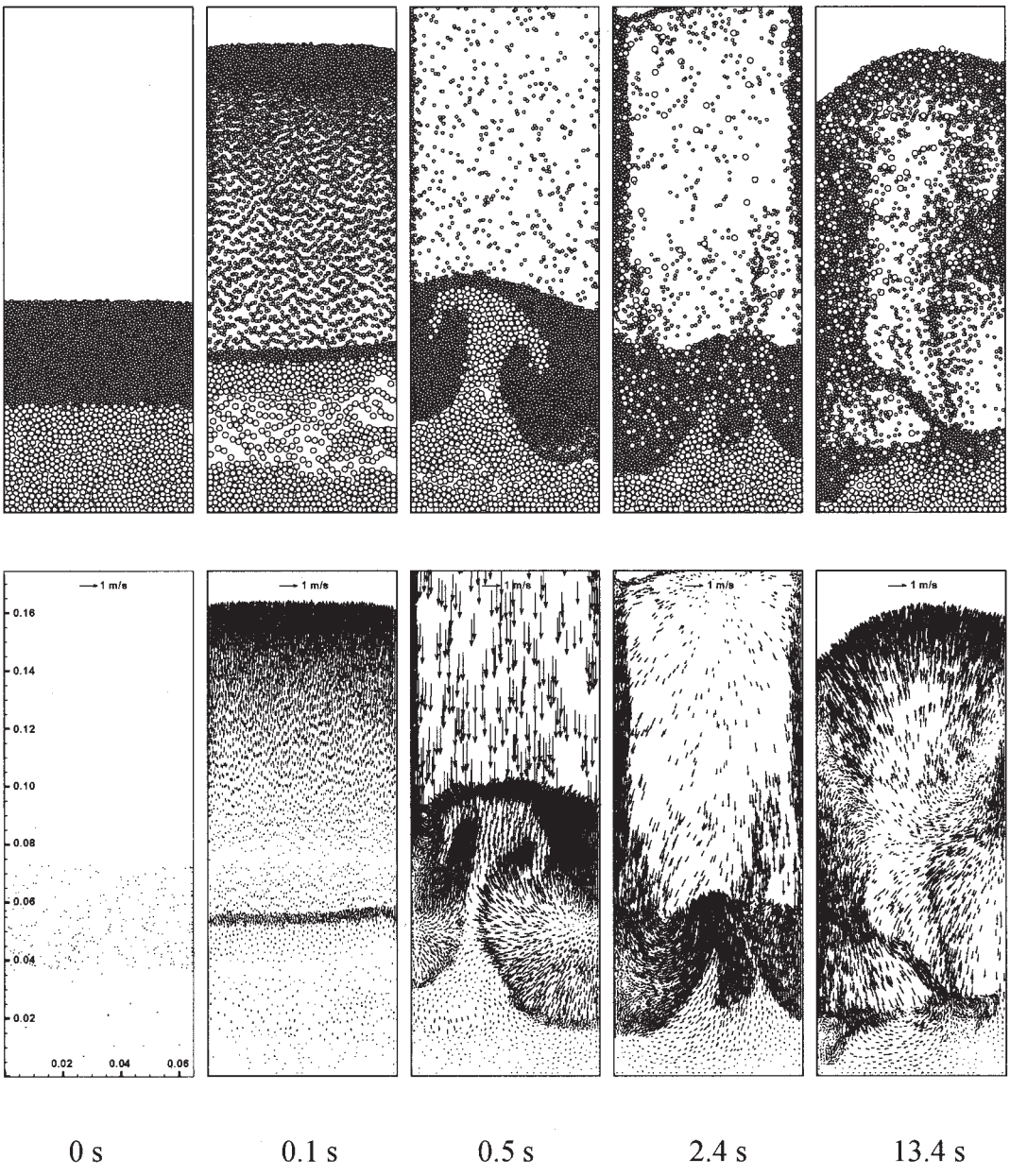

Figure 6. Particle configuration (top) and velocity field (bottom) at different times for a bed whose initial state is fully segregated, when superficial gas velocity is at 1.4 m/s.

$$S_R^2 = \frac{p \cdot q}{N} \tag{7}$$

where p and q are the volume fractions of flotsam and jetsam in a mixture, and N is the equivalent number of particles in the sample. The equation is originally used for monosized particles. For the present binary system, the concept of equivalent particle number is used in the calculation. Each jetsam particle is equivalent to eight flotsam particles, to represent their volume difference. This treatment is equivalent to that suggested by Lacey (1954).

In physical experimentation, sampling is often made from a "frozen" bed, which is produced by a sudden stop of gas flow to allow particles to settle down under gravity, followed by the use of a proper method to divide the whole bed into small sections and measure the concentrations in each section. It is very laborious and suffers a certain deal of uncertainty because of the rearrangements associated with the transition from a fluidized to a fixed bed. Numerical experimentation can avoid this deficiency, given that *in situ* particle information is readily available. However, for gas fluidization, there is still a problem here because the weight of each sample may vary significantly as a result of the presence of bubbles and slugs. Rhodes et al. (2001b) handled this problem by such an approach that while the width of a sample is fixed, its height is adjustable to ensure that each sample has the same number of particles. Although

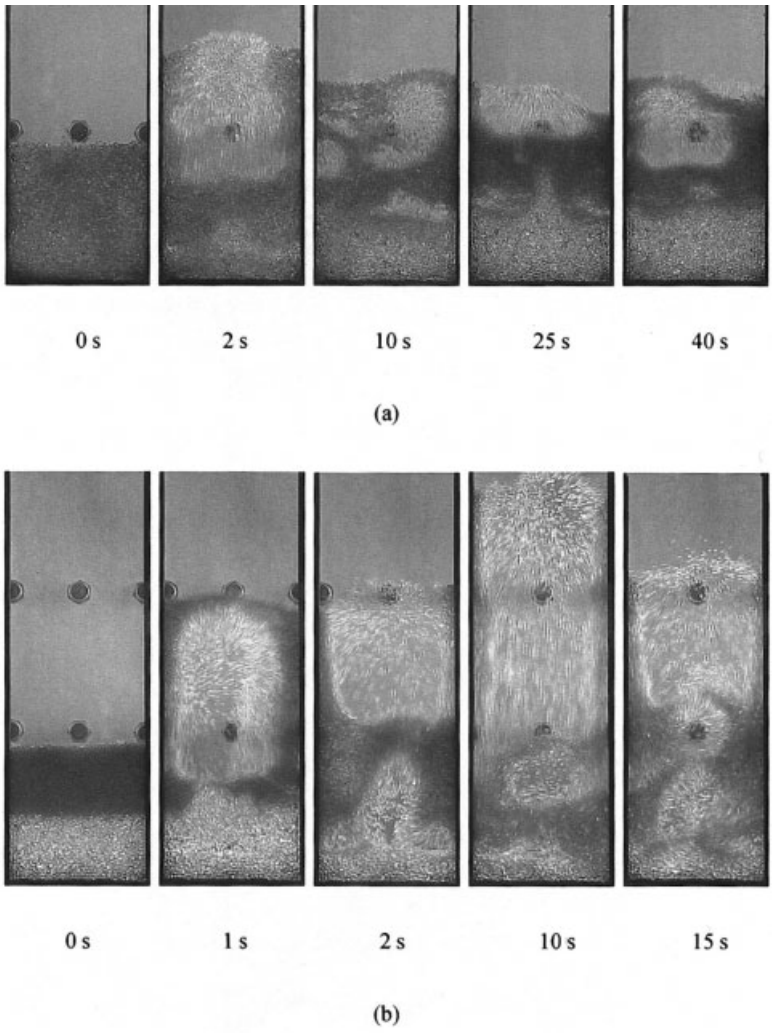

Figure 7. Solid flow patterns observed in the experiment: (a) when v = 1.3 m/s and initial state is well mixed (corresponding to Figure 2); (b) when v = 1.8 m/s and initial state is fully segregated (corresponding to Figure 6).

their method is acceptable for monosized particles, the case they studied, it may experience a limitation when applied to a multisized particle system. Here, we propose an alternative approach that involves the use of a fixed sample size whose contribution to the variance is weighted according to the equivalent number of particles, which varies because of the presence of bubbles, as shown in Figure 8. Thus, variance S^2 is expressed as

$$S^2 = \frac{1}{k_t} \sum_{i=1}^{n} k_{wf}(X_i - \bar{X})^2 \tag{8}$$

where

$$k_t = \sum k_{wf} \tag{9}$$

where k_{wf} is a weighting factor, equal to $N/N_{\max}$ (N is the number of equivalent particles in the ith sample, and $N_{\max}$ is the maximum number of equivalent particles among all the samples at a time step considered), n is the number of samples, X_i is the volume fraction of flotsam in the ith sample, and $\bar{X}$ is the volume fraction of flotsam in the whole bed.

Sample size also affects the value of mixing index as discussed by Fan et al. (1970), for example. If the sample size is too small, down to one particle, the mixing index, even for a well-mixed bed will be zero; if the sample size is too large, up to the bed size, the mixing index will be equal to one even for perfect segregation. Therefore, it is important to find a proper sample size for a considered system. Figure 9 shows the variation of the mixing index with time for three sample sizes from the same case. These sampling sizes are 6.5, 3.25, and 2.167×10^{-3} m and represented by s1, s2, and s3, respectively, in the figure. The same trend can be observed in Figure 9 but the value of mixing index differs for the three sample sizes.

Figure 10 shows the effect of sample size on the mixing index for the two extreme packing states. The results indicate that a sample size between 2.0 to 4.0×10^{-3} m is reasonable,

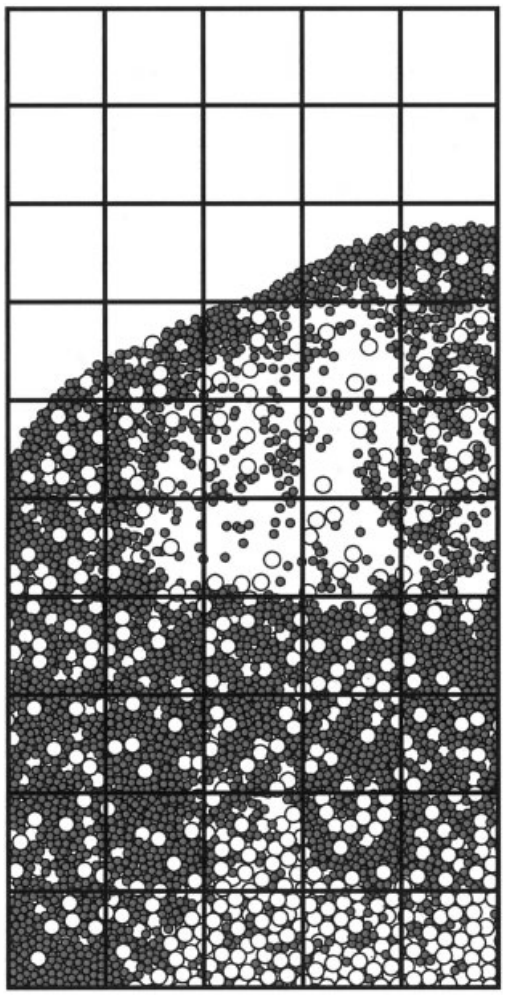

Figure 8. Sampling method used.

satisfying the conditions that the mixing index should be close to one for the well-mixed state and close to zero for the fully separated state. On this basis, the sample size is set to 1/20th of

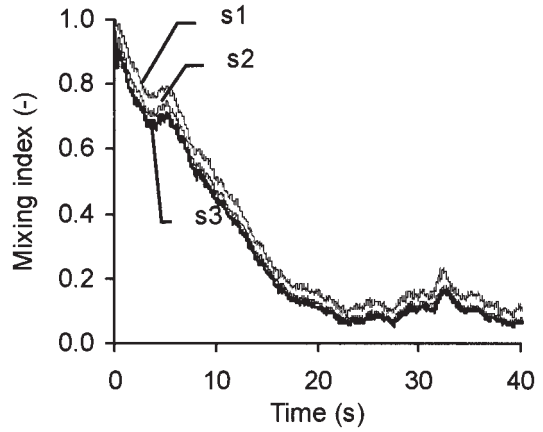

Figure 9. Mixing index as a function of time with different sample sizes (v = 1.0 m/s, and initial state is well mixed): s1, 6.5; s2, 3.25; s3, 2.167 × 10^{-3} m.

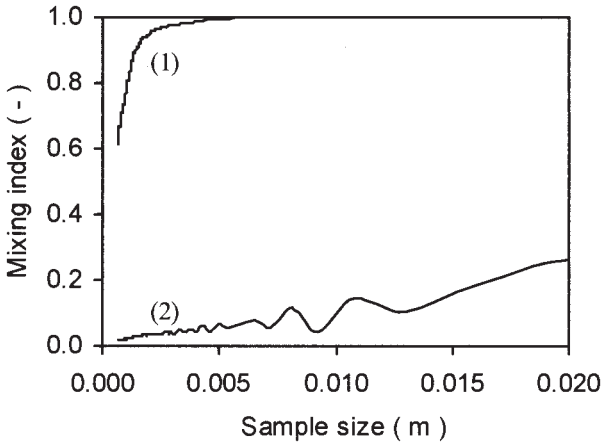

Figure 10. Effect of sample size on mixing index for different packing states: line 1, well mixed; line 2, fully segregated.

the bed width (3.25 × 10^{-3} m) for the present analysis of mixing kinetics.

Figure 11a shows the change of mixing index with time, when the superficial gas velocity is 1.0 m/s. Starting from the perfect mixing state, the mixing index decreases gradually as segregation proceeds. It reaches a value of about 0.1 when the equilibrium state is achieved. On the other hand, starting from the fully segregated state, the mixing index increases as a result of mixing; a similar value is also reached at its equilibrium state. When the superficial gas velocity is 1.4 m/s, as shown in Figure 11b, the mixing indices from two extreme initial conditions reach a similar value, about 0.75, at the equilibrium state. Clearly, it takes a shorter time to reach the equilibrium state at a gas velocity of 1.4 m/s than that at 1.0 m/s. There is also a larger fluctuation at a gas velocity of 1.4 m/s than that at 1.0 m/s. Nevertheless, Figure 11 quantitatively confirms that the final equilibrium state is not sensitive to the initial packing of particles.

Role of particle–particle and particle–fluid interactions

The flow and segregation of particles in a fluidized bed is controlled by the interactions between particles, between particles and fluid, and between particles and wall, in addition to the gravitational force. The analysis of these interaction forces is therefore key to developing a better understanding of the underlying mechanisms. Such information is very difficult, if not impossible, to obtain fully with the current experimental techniques, but is readily available from the present DPM-CFD study. Figure 12 shows the spatial distributions of velocity and force fields when the initial condition is well mixed and gas injection velocity is 1.4 m/s after 3.5 s of simulation. The magnitudes of these forces acting on a particle are nondimensionized by its gravity force. As can be seen from Figure 12a, large contact forces are found mainly in the area where particles are crowded and the relative velocity between particles is high, and the value can be hundreds of times of its weight. On the other hand, Figures 12b and 12c show that the drag force in a dense area is larger than that in a loose area, both horizontally and vertically, because of the difference in porosity and permeability. Drag force is generally greater in the vertical direc-

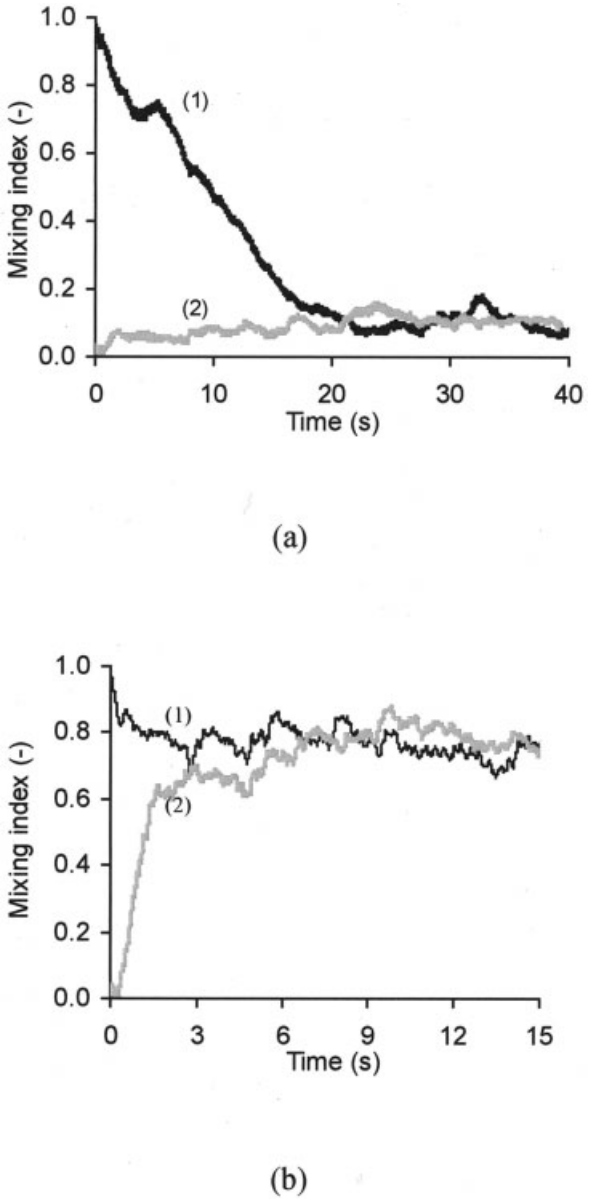

Figure 11. Mixing index as function of time for different initial states at different superficial gas velocities: (a) v = 1.0 m/s; (b) v = 1.4 m/s; line 1, well mixed; line 2, fully segregated.

tion than in the horizontal direction and is low near the wall. The particle–particle and particle–fluid interactions are strong. As a consequence, as shown in Figure 12d, vigorous particle motion is observed, producing good mixing, as shown in Figure 11b.

The particle–particle and particle–fluid interaction forces vary not only spatially but also temporally. To highlight this point, Figure 13 shows the variation of the spatial distribution of the drag forces acting on individual particles and velocity distribution with time when the initial condition is well mixed and gas injection velocity is 1.0 m/s. Because segregation takes place mainly in a vertical direction, the present analysis of the drag force is focused on the vertical component only. It can be seen that, at t = 1.5 s, jetsam particles accumulate in the lower part of the bed, and a big bubble bursts out in the upper part, whereas a bubble forms at the interface between flotsam and jetsam. In general, the upward drag force acting on the flotsam particles is greater than that on the surrounding jetsam particles, noting that the drag force of a particle is again nondimensionized by its own gravity. This difference produces separation of flotsam and jetsam in the loose regions, such as the top bubbling region and the bottom bubble-initiating region. In the middle dense region, the drag force on a flotsam particle is greater than its gravity, whereas the drag force on a jetsam particle is less than its gravity. However, because there is no space for the rearrangement of particles in this region, the jetsam particles are lifted up by their underneath flotsam particles, producing a mixing process. Particles lifted up by a bubble will fall down once the drag force cannot balance the gravity. The falling mainly occurs to particles close to the walls, where the drag force is small and, combined with the rising of particles in the center, generates dual vortices. Bubble formation, rising, and bursting out are repetitive, and so are the rising and falling of particles. A macroscopically stable state can be reached when the mixing is balanced by the segregation associated with the repetitive processes.

Obviously, the mixing/segregation process is very complicated. Detailed analysis of the gas and solid flow in relation to the particle–particle and particle–fluid interaction forces based on the DPM-CFD results may offer a way to generate an ultimate answer to the question of how and why segregation/mixing occurs in gas fluidization. Such studies largely represent our present ongoing research effort. In the meantime, simply by examining the time- and space-averaged results, we found that the segregation and mixing phenomena observed can be reasonably explained, as discussed below.

By definition, at a given time, the mean drag force on a particle is calculated as

$$\frac{1}{N_p}\sum_{i=1}^{N_p}\mathbf{f}_{f,i}$$

where N_p is the number of one type of particles (flotsam or jetsam). The mean interparticle interaction force on a particle, which includes the contact force and damping force, is calculated as

$$\frac{1}{N_p}\sum_{i=1}^{N_p}\left[\sum_{j=1}^{k_i}(\mathbf{f}_{cn,ij}+\mathbf{f}_{dn,ij}+\mathbf{f}_{ct,ij}+\mathbf{f}_{dt,ij})\right]$$

The mean interaction force between particles and walls can be defined similarly. Because segregation occurs in a vertical direction, our analysis is again focused on the forces in this direction for simplicity. Figure 14 shows the variation of the mean fluid drag force, particle–particle interaction force, and particle–wall interaction force (nondimensionized by their respective gravity force) with time, when the initial condition is well mixed and gas injection velocity is 1.0 m/s. At the start of gas injection, the upward fluid drag force is greater than the gravity force for flotsam (Figure 14a) and

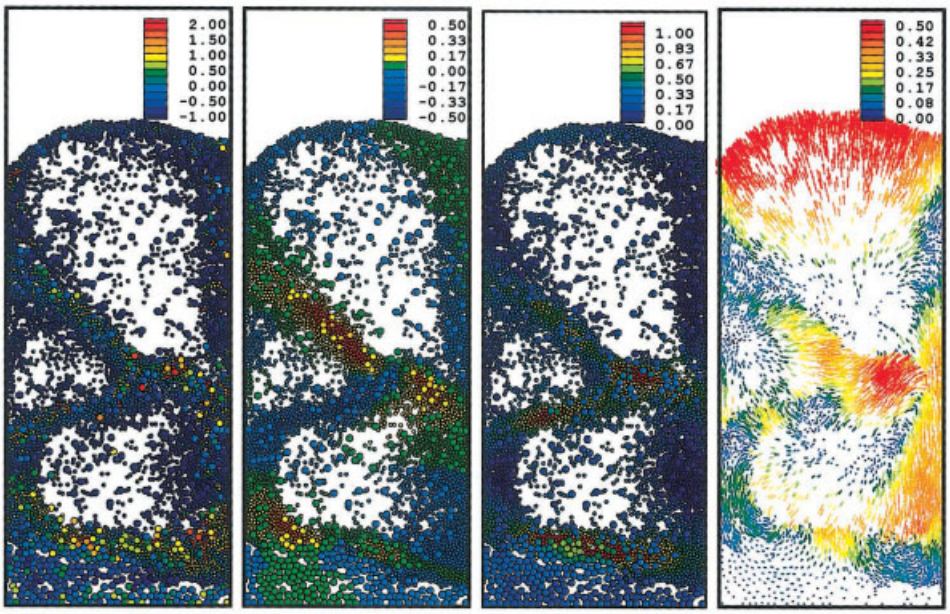

Figure 12. Snapshots showing the spatial distribution of forces and velocities when $t = 3.5$ s, $v = 1.4$ m/s, initial state is well mixed: (a) particle–particle contact force in logarithmic scale; (b) fluid drag force in horizontal direction; (c) fluid drag force in vertical direction; (d) particle velocity.

less than the gravity force for jetsam (Figure 14b). This will provide a driving force for segregation, with flotsam rising to the top and the jetsam sinking to the bottom of the bed. On the other hand, the resulting upward motion of flotsam particles and the downward flow of jetsam particles are hindered by the particle–particle interaction forces from their surrounding particles. The particle–wall interaction force is small because the gravity is mainly supported by the fluid drag force, although this force acting on jetsam particles fluctuates more significantly than that on flotsam particles. Two stages can be identified from Figure 14: transient stage and stable stage. At the transient stage, the drag force decreases for flotsam and increases for jetsam. This should correspond to the rearrangement and segregation process of particles in the bed. Consequently, the interaction force between flotsam and jetsam decreases. After about 20 s, the forces simply fluctuate around their mean values, and a macroscopically stable stage is reached. At this stage, flotsam is rich in the top part of the bed and remains in a fluidized state, and jetsam is rich in the bottom part and remains in a defluidized state. These two stages are consistent with the mixing kinetics quantified by the mixing index in Figure 11a.

When the gas injection velocity is increased to 1.4 m/s, the patterns of these interaction forces differ and these forces fluctuate more vigorously, as shown in Figure 15. Although starting from the same initial packing condition, the transient stage is very short, only about 2 s. Note that the time in this figure is expressed in logarithmic scale to better illustrate the transient stage. It can be seen that the drag force on flotsam or jetsam particles is much greater than their gravity when gas injection starts, yielding fluidization of the whole bed (Figure 3) and good mixing (Figure 11). At the stable state, the drag forces simply fluctuate around their respective mean values (1.27 for flotsam and 0.66 for jetsam). Interestingly, the mean drag force for jetsam particles is much smaller than their gravity force. Hence, the fluidization of jetsam must be achieved by a strong interaction between flotsam and jetsam, which is indeed the case. As shown in Figure 15, there is a strong interaction force between flotsam and jetsam to lift up the jetsam particles. For flotsam, this force is downward, to counteract the upward drag force, to establish a macroscopically stable flow. Therefore, if the small particle–wall interaction force, which supports jetsam particles sitting on the bottom wall, is taken into account, the overall forces on the whole bed are balanced.

Conclusions

A DPM-CFD model was developed and validated to study the segregation and mixing of binary mixtures of particles in a gas-fluidized bed where the motion of individual particles is 3-D and the flow of continuous gas is 2-D. The results from the present work can be summarized as follows:

(1) For a given fluidized system, the degree of mixing/segregation is strongly affected by gas velocity. Significant segregation occurs when gas velocity can fluidize only flotsam but not jetsam, and reasonably satisfactory mixing occurs when gas injection velocity is strong enough to fluidize the whole bed. The initial packing state of particles affects the segregation/mixing kinetics but not the final equilibrium state at a given gas velocity. These results are qualitatively comparable

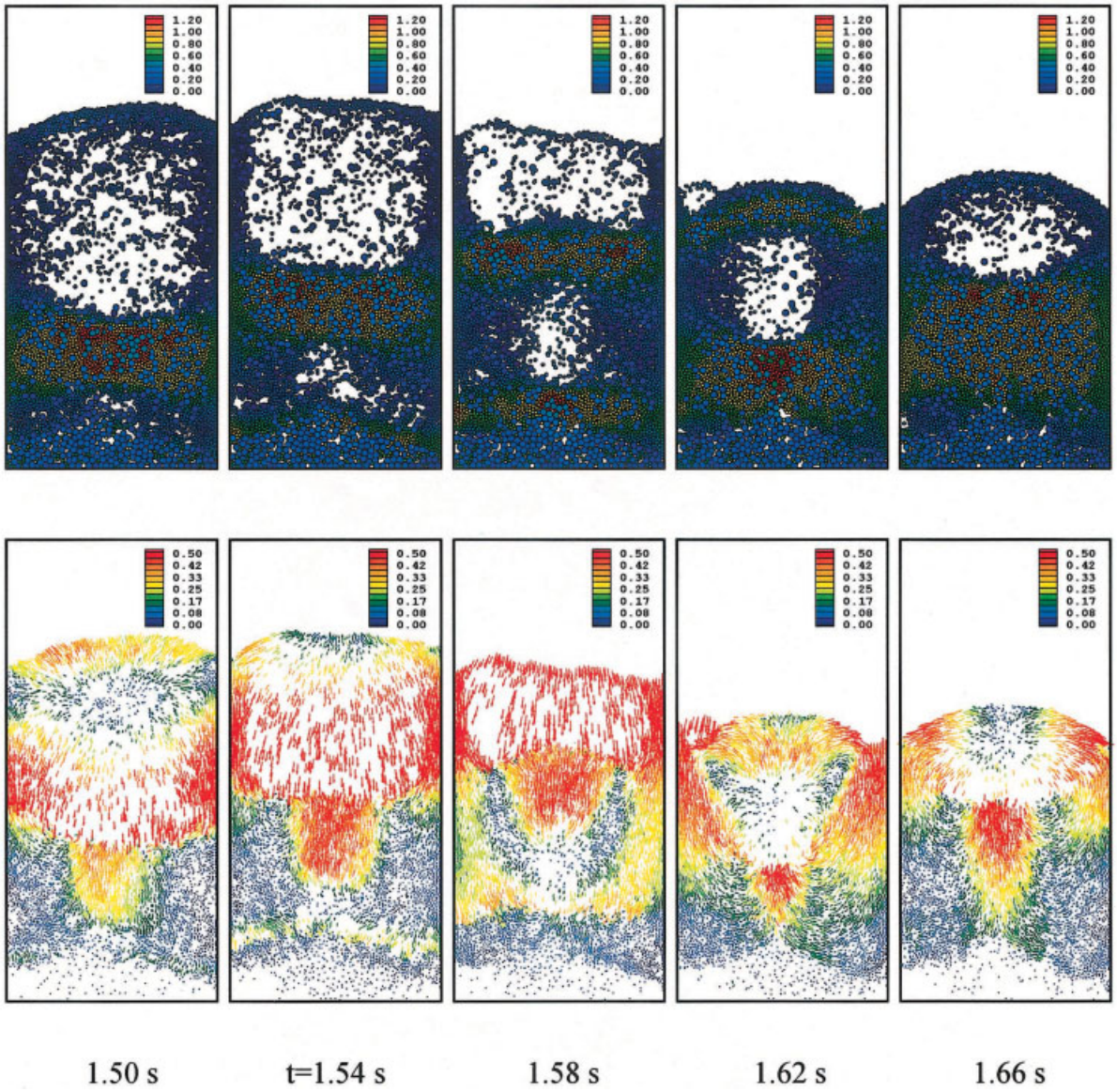

Figure 13. Transition of the spatial distribution of vertical drag force (top) and velocity (bottom) when v = 1.0 m/s and the initial state is well mixed.

with the physical experiments conducted under similar conditions in terms of flow patterns, confirming the validity of the proposed method.

(2) The segregation/mixing process was analyzed under dynamic conditions. A weighted Lacey mixing index was proposed to quantify the mixing kinetics. The effect of sample size on the mixing index is examined based on the numerical results. It is proposed that an appropriate sampling size should be able to describe properly the two extremes: well mixed and fully segregated. Segregation associated with the defluidization of jetsam is a gradual process, whereas mixing of jetsam and flotsam in fluidization can be achieved rapidly.

(3) Mechanisms of mixing/segregation process were studied in terms of interaction forces between particles and between particles and fluids. It is shown that these forces vary not only temporally but also spatially, phenomena that will need more detailed analysis in future investigations. However, focused on the vertical components of these forces, the present results demonstrate that particle segregation occurs as a result of the strong fluid drag force lifting the flotsam before a dynamical equilibrium state is reached. The particle–particle interaction, like the particle–fluid interaction, plays an important role in achieving uniform fluidization.

Notation

$C_{d0,i}$ = drag coefficient on an isolated particle i, dimensionless
E = Young's modulus, $N \cdot m^{-2}$
$\mathbf{f}$ = contact, drag, or gravitational force, N
$\mathbf{F}$ = volumetric fluid–particle interaction force, $N \cdot m^{-3}$
g = gravitational acceleration, ms^{-2}
I = rotational inertia momentum of particle, kg/m^2
k_c = number of particles in a computational cell, dimensionless
k_f = sample numbers after weighting process, dimensionless
k_i = number of particles in contact with i, dimensionless
k_{wf} = weighting factor of a sample, dimensionless

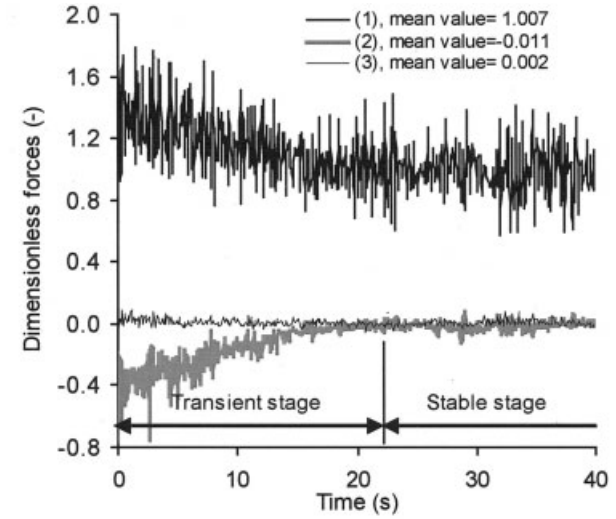

(a)

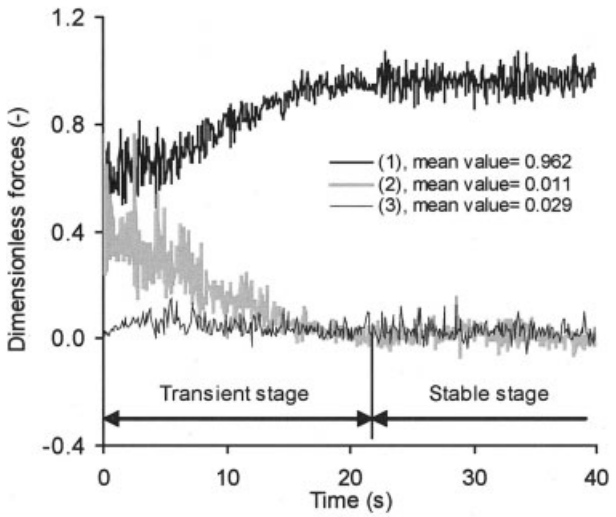

(b)

Figure 14. Variation of mean interaction forces with time at vertical direction when gas velocity is 1.0 m/s and the initial state is well mixed.

(a) Flotsam; (b) jetsam; line 1, particle–fluid interaction force; line 2, particle–particle interaction force; line 3, particle–wall interaction force.

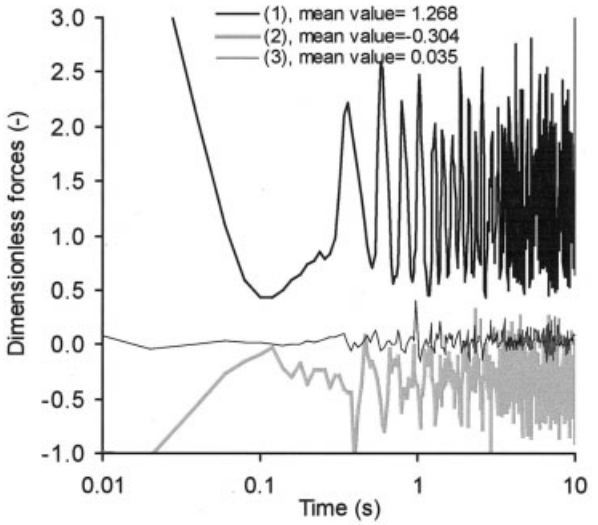

(a)

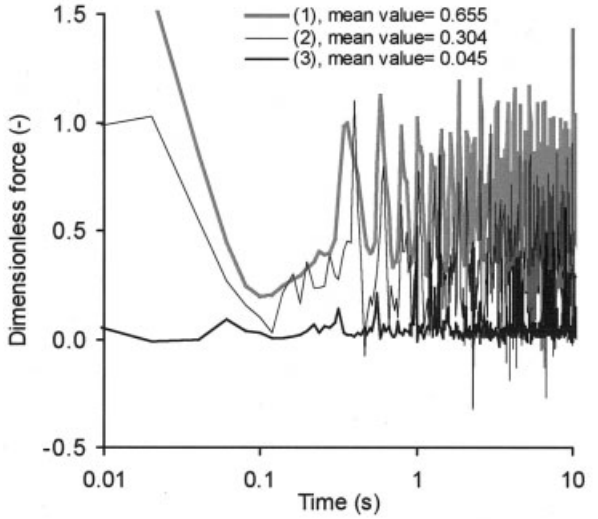

(b)

Figure 15. Variation of mean interaction forces with time at vertical direction when gas velocity is 1.4 m/s and the initial state is segregated.

(a) Flotsam; (b) jetsam; line 1, particle–fluid interaction force; line 2, particle–particle interaction force; line 3, particle–wall interaction force.

m = mass, kg
M = mixing index, dimensionless
n = number of samples, dimensionless
N = number of particles in each sample, dimensionless
N_p = total number of particles having same size, dimensionless
P = pressure, Pa
p = concentration of flotsam in a mixture, dimensionless
q = concentration of jetsam in a mixture, dimensionless
R_i = particle radius, m
$\mathbf{R}_i$ = vector of magnitude R_i from the mass center of particle i to a contact point, m
$Re_{p,i}$ = Reynolds number of particle i, dimensionless
S_0^2 = variance at totally segregated condition, dimensionless
S_R^2 = variance at random mixed condition, dimensionless
S^2 = the actual variance, dimensionless
t = time, s
T = torque, N·m
$\mathbf{u}$ = gas velocity, m/s
$\mathbf{v}$ = solid velocity, m/s
V = volume, m^3
ΔV = volume of computational cell, m^3
$\bar{X}$ = concentration of flotsam in the whole bed, dimensionless
X_i = concentration of flotsam on the ith sample, dimensionless

Greek letters

$\delta_{t,ij}$ = vector of the accumulated tangential displacement between particles i and j, m
ϵ = porosity, dimensionless
$\eta_{n,\eta t}$ = normal and tangential damping coefficients, respectively, dimensionless

μ = viscosity, kg m^{-1} s^{-1}
ν = Poisson ratio, N·m^{-1}
ρ = density, kg/m^3
$\boldsymbol{\tau}$ = continuum phase viscous stress tensor, kg m^{-1} s^{-2}
$\boldsymbol{\omega}$ = rotational velocity of particle, s^{-1}

Subscripts

c = contact
d = damping
f = fluid phase
i = particle i
j = particle j
p = particle

Acknowledgments

The authors are grateful to the Australia Research Council and BHP Steel for the financial support of this work.

Literature Cited

Beeckmans, J. M., "Segregation Mechanisms in Gas Fluidized Beds," *Chem. Eng. J.*, **28**, 1 (1984).
Cundall, P. A., and O. D. L. Strack, "A Discrete Numerical Model for Granular Assemblies," *Geotechnique*, **29**, 47 (1979).
Di Felice, R., "The Voidage Function for Fluid–Particle Interaction Systems," *Int. J. Multiphase Flow*, **20**, 153 (1994).
Fan, L. T., S. J. Chen, and C. A. Watson, "Solid Mixing," *Ind. Eng. Chem.*, **62**, 53 (1970).
Formisani, B., G. D. Cristofaro, and R. Girimonte, "A Fundamental Approach to the Phenomenology of Fluidization of Size Segregation Binary Mixtures of Solids," *Chem. Eng. Sci.*, **56**, 109 (2001).
Gibilaro, L. G., and P. N. Rowe, "A Model for a Segregating Gas Fluidized Bed," *Chem. Eng. Sci.*, **29**, 1403 (1974).
Gidaspow, D., *Multiphase Flow and Fluidization*, Academic Press, San Diego, CA (1994)
Helland, E., R. Occelli, and L. Tadrist, "Numerical Study of Cluster Formation in a Gas-Particle Circulating Fluidized Bed," *Powder Technol.*, **110**, 210 (2000).
Hemiti, M., K. Spieker, C. Laguerie, R. Alvarez, and F. A. Riera, "Experimental Study of Sawdust and Coal Particle Mixing in Sand or Catalyst Fluidized Beds," *Can. J. Chem. Eng.*, **68**, 768 (1990).
Hoffmann, A. C., L. P. B. M. Janssen, and J. Prins, "Particle Segregation in Fluidised Binary Mixtures," *Chem. Eng. Sci.*, **48**, 1583 (1993).
Hoomans, B. P. B., J. A. M. Kuipers, M. A. Mohd Salleh, M. Stein, and J. P. K. Seville, "Experimental Validation of Granular Dynamics Simulations of Gas-Fluidised Beds with Homogenous In-Flow Conditions Using Positron Emission Particle Tracking," *Powder Technol.*, **116**, 166 (2001).
Hoomans, B. P. B., J. A. M. Kuipers, and W. P. M. Van Swaaij, "The Influence of Particle Properties on Pressure Signals in Dense Gas-Fluidized Beds: A Computer Simulation Study," *Proc. 3rd World Congress on Particle Technology*, Brighton, UK, p. 213 (1998).
Hoomans, B. P. B., J. A. M. Kuipers, and W. P. M. Van Swaaij, "Granular Dynamics Simulation of Segregation Phenomena in Bubbling Gas-Fluidised Beds," *Powder Technol.*, **109**, 41 (2000).
Kafui, K. D., C. Thornton, and M. J. Admas, "Discrete Particle-Continuum Fluid Modelling for Gas–Solid Fluidised Beds," *Chem. Eng. Sci.*, **57**, 2395 (2002).
Kaneko, Y., T. Shiojima, and M. Horio, "DEM Simulation of Fluidized Beds for Gas-Phase Olefin Polymerization," *Chem. Eng. Sci.*, **54**, 5809 (1999).
Kawaguchi, T., M. Sakamoto, T. Tanaka, and Y. Tsuji, "Quasi-Three-Dimensional Numerical Simulation of Spouted Beds in Cylinder," *Powder Technol.*, **109**, 3 (2000).
Kawaguchi, T., and Y. Tsuji, "Numerical Simulation of Two-Dimensional Fluidized Beds Using the Discrete Element Method (Comparison between the Two- and Three-Dimensional Models)," *Powder Technol.*, **96**, 129 (1998).
Kuwagi, K., T. Mikami, and M. Horio, "Numerical Simulation of Metallic Solid Bridging Particles in a Fluidised Bed at High Temperature," *Powder Technol.*, **109**, 27 (2000).
Lacey, P. M. C., "Developments in the Theory of Particle Mixing," *J. Appl. Chem.*, **4**, 257 (1954).
Li, J., and J. A. M. Kuipers, "Effect of Pressure on Gas–Solid Flow Behavior in Dense Gas-Fluidized Beds: A Discrete Particle Simulation Study," *Powder Technol.*, **127**, 173 (2002).
Li, J., and D. J. Mason, "A Computational Investigation of Transient Heat Transfer in Pneumatic Transport of Granular Particles," *Powder Technol.*, **112**, 273 (2000).
Mikami, T., H. Kamiya, and M. Horio, "Numerical Simulation of Cohesive Powder Behavior in a Fluidized Bed," *Chem. Eng. Sci.*, **53**, 1927 (1998).
Nienow, A. W., P. N. Rowe, and L. Y. L. Cheung, "A Quantitative Analysis of the Mixing of Two Segregating Powders of Different Density in a Gas-Fluidised Bed," *Powder Technol.*, **20**, 89 (1978).
Nienow, A. W., N. S. Naimer, and T. Chiba, "Studies of Segregation/Mixing in Fluidised Beds of Different Size Particles," *Chem. Eng. Commun.*, **62**, 53 (1987).
Ouyang, J., and J. Li, "Discrete Simulation of Heterogeneous Structure and Dynamic Behavior in Gas–Solid Fluidization," *Chem. Eng. Sci.*, **54**, 5427 (1999).
Poux, M., P. Fayolle, J. Bertrand, D. Bridoux, and J. Bousquet. "Powder Mixing: Some Practical Rules Applied to Agitated Systems," *Powder Technol.*, **68**, 213 (1991).
Rhodes, M. J., X. S. Wang, M. Ngyen, P. Stewart, and K. Liffman, "Use of Discrete Element Method Simulation in Studying Fluidization Characteristics: Influence of Interparticle Force," *Chem. Eng. Sci.*, **56**, 69 (2001a).
Rhodes, M. J., X. S. Wang, M. Ngyen, P. Stewart, and K. Liffman, "Study of Mixing in Gas-Fluidized Beds Using a DEM Model," *Chem. Eng. Sci.*, **56**, 2859 (2001b).
Rice, R. W., and J. F. Brainovich, "Mixing/Segregation in Two- and Three-Dimensional Fluidized Bed: Binary Systems of Equidensity Spherical Particles," *AIChE J.*, **32**, 35 (1986).
Rollins, D. K., D. L. Faust, and D. L. Jabas, "A Superior Approach to Indices in Determining Mixture Segregation," *Powder Technol.*, **84**, 277 (1995).
Rong, D., T. Mikami, and M. Horio, "Particle and Bubble Movements around Tubes Immersed in Fluidized Beds—A Numerical Study," *Chem. Eng. Sci.*, **54**, 5737 (1999).
Rowe, P. N., A. W. Nienow, and A. J. Agbim, "The Mechanisms by Which Particles Segregate in Gas Fluidised Beds—Binary Systems of Near-Spherical Particles," *Trans. IChemE*, **50**, 310 (1972).
Shen, L., and M. Zhang, "Effect of Particle Size on Solids Mixing in Bubbling Fluidized Beds," *Powder Technol.*, **97**, 170 (1998).
Stein, M., J. Seville, D. Parker, and D. Allen, "Scale-up of Particle Motion in Fluidised Beds Using Position Emission Particle Tracking," *Fluidization—IX*, L. S. Fan and T. M. Knowlton, eds., Engineering Foundation, New York (1998).
Stewart, R., J. Bridgwater, Y. C. Zhou, and A. B. Yu, "Simulated and Measured Flow of Granules in a Bladed Mixer—A Detailed Comparison," *Chem. Eng. Sci.*, **56**, 5457 (2001).
Thornton, C., ed., "Numerical Simulation of Discrete Particle Systems," *Powder Technol.*, **209** [a special issue containing many relevant papers] (2000).
Tsuji, Y., T. Kawaguchi, and T. Tanaka, "Discrete Particle Simulation of Two-Dimensional Fluidized Bed," *Powder Technol.*, **77**, 79 (1993).
Wu, S. Y., and J. Baeyens, "Segregation by Size Difference in Gas Fluidized Beds," *Powder Technol.*, **98**, 139 (1998).
Xu, B. H., and A. B. Yu, "Numerical Simulation of the Gas–Solid Flow in a Fluidised Bed by Combining Discrete Particle Method with Computational Fluid Dynamics," *Chem. Eng. Sci.*, **52**, 2786 (1997).
Xu, B. H., and A. B. Yu, "Numerical Study of the Forces Acting on Individual Particles in Gas Fluidised Beds," *Fluidisation—IX*, L. S. Fan and T. M. Knowlton, eds., Engineering Foundation, New York (1998).
Xu, B. H., and A. B. Yu, "A New Stability Criterion of Gas Fluidization," *World Congress on Particle Technology*, Vol. 4, July 21–25, Sydney, Australia (2002).
Xu, B. H., A. B. Yu, S. J. Chew, and P. Zulli, "Simulation of the Gas–Solid Flow in a Bed with Lateral Gas Blasting," *Powder Technol.*, **109**, 14 (2000).
Xu, B. H., A. B. Yu, and P. Zulli, "The Effect of Interparticle Forces on Powder Fluidization Behaviour," *Powders and Grains*, Y. A. A. Kishino, ed., Balkema, Rotterdam, The Netherlands, pp. 577–580 (2001).

Yang, R.Y., R. P. Zou, and A. B. Yu, "Computer Simulation of the Packing of Fine Particles," *Phys. Rev. E*, **62**, 3900 (2000).
Yu, A. B., "Discrete Element Method—An Effective Method for Particle Scale Research of Particulate Matter," *Proc. 3rd Int. Conf. on DEM*, B. K. Cook and R. P. Jensen, eds., ASCE Geotechnical Special Publication No. 117, pp. 17–22 (2002).
Yu, A. B., and B. H. Xu, "Particle Scale Modelling of Particle–Fluid Flow in Fluidization," *J. Chem. Technol. Biotechnol.*, **78**, 111 (2003).
Yuu, S., T. Umekage, and Y. Johno, "Numerical Simulation of Air and Particle Motions in Bubbling Fluidized Bed of Small Particles," *Powder Technol.*, **110**, 158 (2000).
Zhang, S. J., and A. B. Yu, "Computational Investigation of Slugging Phenomena in Gas Fluidization," *Powder Technol.*, **123**, 147 (2002).
Zhang, S. J., A. B. Yu, B. Wright, P. Zulli, and U. Tuzun, "Modelling of the Granular Flow in a Blast Furnace," *ISIJ Int.*, **38**, 1311 (1998).

Manuscript received Apr. 8, 2003, revision received Sep. 12, 2003, and final revision received Dec. 18, 2003.